Influence of Polymorphism on the Surface Energetics of Salmeterol Xinafoate Crystallized from Supercritical Fluids

Henry H. Y. Tong,[1] Boris Yu. Shekunov,[2,3] Peter York,[2,3] and Albert H. L. Chow[1,4]

Received January 14, 2002; accepted February 4, 2002

Purpose. To characterize the surface thermodynamic properties of two polymorphic forms (I and II) of salmeterol xinafoate (SX) prepared from supercritical fluids and a commercial micronized SX (form I) sample (MSX).

Methods. Inverse gas chromatographic analysis was conducted on the SX samples at 30, 40, 50, and 60°C using the following probes at infinite dilution: nonpolar probes (NPs; alkane C5–C9 series); and polar probes (PPs; i.e., dichloromethane, chloroform, acetone, ethyl acetate, diethyl ether, and tetrahydrofuran). Surface thermodynamic parameters of adsorption and Hansen solubility parameters were calculated from the retention times of the probes.

Results. The free energies of adsorption ($-\Delta G_A$) of the three samples obtained at various temperatures follow this order: SX-II > MSX ≈ SX-I for the NPs; and SX-II > MSX > SX-I for the PPs. For both NPs and PPs, SX-II exhibits a less negative enthalpy of adsorption (ΔH_A) and a much less negative entropy of adsorption (ΔS_A) than MSX and SX-I, suggesting that the high $-\Delta G_A$ of SX-II is contributed by a considerably reduced entropy loss. The dispersive component of surface free energy (γ_s^D) is the highest for MSX but the lowest for SX-II at all temperatures studied, whereas the specific component of surface free energy of adsorption ($-\Delta G_A^{SP}$) is higher for SX-II than for SX-I. That SX-II displays the highest $-\Delta G_A$ for the NP but the lowest γ_s^D of all the SX samples may be explained by the additional $-\Delta G_A$ change associated with an increased mobility of the probe molecules on the less stable and more disordered SX-II surface. The acid and base parameters, K_A and K_D, that were derived from ΔH_A^{SP} reveal significant differences in the relative acid and base properties among the samples. The calculated Hansen solubility parameters (δ_D, δ_P, and δ_H) indicate that the surface of SX-II is the most polar and most energetic of all the three samples in terms of specific interactions (mostly hydrogen bonding).

Conclusions. The metastable SX-II polymorph possesses a higher surface free energy, higher surface entropy, and a more polar surface than the stable SX-I polymorph.

KEY WORDS: supercritical fluid crystallization; salmeterol xinafoate polymorphs; inverse gas chromatography; surface energetics; Hansen solubility parameters.

INTRODUCTION

In recent years, the application of supercritical fluid technologies in the controlled production of microfine drug powders with the desired physical and surface properties for pulmonary delivery has received considerable attention in the pharmaceutical industry. Of particular promise in this latest development is the solution-enhanced dispersion by supercritical fluid (SEDS) technology.

Compared with the traditional approach to fine powder production employing sequential batch crystallization and fluid energy milling, the SEDS process offers the special advantage that micron-sized particles can be produced in a highly pure, crystalline, noncohesive, and solvent-free form of fairly uniform size in a single-step operation (1–3). In addition, the physical and surface properties as well as the crystal forms of the drugs all can be regulated simply by varying the SEDS operating parameters (3,4). This attractive capability of the SEDS process has been demonstrated for salmeterol xinafoate (SX), a highly selective, long-acting β_2-adrenergic bronchodilator, which can be reproducibly crystallized in two physically pure polymorphic forms (SX-I and SX-II) through appropriate adjustment of the operating temperature and pressure of the process (3). Solubility and differential scanning calorimetric studies confirmed that these two polymorphs are enantiotropically related, with SX-I being the thermodynamically stable form at ambient temperature and pressure (5). Surface analysis of the two SEDS-processed polymorphs at 40°C by inverse gas chromatography (IGC) revealed that SX-I has a larger dispersive component of surface free energy (determined by nonpolar probe [NP]), γ_S^D, than does SX-II, while the specific component of surface free energy of adsorption, $-\Delta G_A^{SP}$, of SX-II is larger than that of SX-I for all the polar probes (PPs) employed (5). Comparison of the SEDS-processed SX-I with a reference micronized commercial SX sample (MSX) of grossly identical crystal structure indicated that the SEDS sample has a smaller γ_S^D and $-\Delta G_A^{SP}$, which is consistent with its thermodynamically more stable surface structure. The acidity and basicity constants, K_A and K_D, which reflect the acid and base properties of the surface, also exhibit a larger magnitude for SX-II than for SX-I. The relatively high surface free energy for specific interactions and the large K_A and K_D values of SX-II have been attributed to its polar acidic (OH and COOH) and basic (NH) groups being more exposed than the nonpolar bulky groups (i.e., benzene and naphthalene) at the crystal surface. It should be noted, however, that, as has been a common practice in the pharmaceutical field, these K_A and K_D values were calculated from ΔG_A^{SP} instead of ΔH_A^{SP}, based on the assumption of negligible contribution of ΔS_A^{SP}. As an extension of the aforementioned IGC studies on the SX polymorphs, the present investigation carries the following two objectives: to verify the validity of this assumption; and to further probe the surface energy differences between the two SX forms. To this end, the enthalpic and entropic adsorption thermodynamic properties as well as the Hansen solubility parameters of the samples have been determined by IGC analysis at various temperatures. These thermodynamic measurements afford a simple approach to quantifying the cohesive and adhesive properties of materials and may be useful

[1] School of Pharmacy, The Chinese University of Hong Kong, 6/F, Rm 616, Basic Medical Sciences Building Shatin, New Territories, Hong Kong SAR, China.

[2] Bradford Particle Design plc, Unit 49 Listerhills Science Park, Campus Road, Bradford BD7 1HR, United Kingdom.

[3] Drug Delivery Group, School of Pharmacy, University of Bradford, Bradford BD7 1DP, United Kingdom.

[4] To whom correspondence should be addressed. (e-mail albert-chow@cuhk.edu.hk)

0724-8741/02/0500-0640/0

for predicting the surface-related dispersibility and aerosol performance of the SEDS-processed SX polymorphs (6).

MATERIALS AND METHODS

Chemicals and Reagents

The sources and grades of all materials, chemicals, and solvents employed as well as the preparation procedure for the SEDS-processed SX samples (SX-I and SX-II) have been reported previously (5).

Surface Analysis by IGC

IGC analysis at infinite dilution was conducted on each SX sample (MSX, SX-I, and SX-II) at 30, 40, 50, and 60°C, as previously described (5) using a Hewlett Packard Series II 5890 Gas Chromatograph (Wilmington, Delaware) equipped with an integrator and flame ionization detector. Surface thermodynamic parameters of adsorption and Hansen solubility parameters were calculated from the retention times of the probes as detailed in the following section. All determinations were performed in triplicate.

THEORY AND CALCULATIONS

Standard Free Energy of Adsorption and Related Thermodynamic Parameters

The experimental parameter measured in IGC for the adsorption of probes on the stationary phase (i.e., SX sample) inside the glass columns is the retention time of the probes, which can be converted to the retention volume by the following relationship (7):

$$V_N = j.F.(t_r - t_0) \quad (1)$$

where V_N is the net retention volume, j is a correction factor taking into account gas compressibility, F is the carrier gas flow rate, t_r is the retention time of the probe, and t_0 is the void retention time.

The standard free energy of adsorption, ΔG_A, of the probe on the SX sample can be calculated from V_N using the following relationship (7):

$$-\Delta G_A = RT \ln (V_N P_0 / SgB_0) \quad (2)$$

where T is the column temperature, R is the gas constant, P_0 is the reference partial pressure of the probe, S is the specific surface area of the sample, g is the weight of sample, and B_0 is the reference bidimensional spreading pressure of the adsorbed probe film on the sample. In the present study, ΔG_A was calculated using the reference state of de Boer (8), where $P_0 = 1.013 \times 10^5$ Pa and $B_0 = 3.38 \times 10^{-4}$ Nm^{-1}.

Equation (2) also may be expressed in the following form:

$$-\Delta G_A = RT \ln V_N + C \quad (3)$$

where C is a constant encompassing the choice of the standard state for ΔG_A and the surface area of the sample.

To a first approximation, the free energy of adsorption is related to the work of adhesion, W_A, by the following equation:

$$-\Delta G_A = N.a.W_A + K \quad (4)$$

where N is the Avogadro's number, a is the surface area of probe, and K is a constant that has been introduced to account for the choice of the standard state of ΔG_A.

The surface free energy of adsorption (ΔG_A) can be related to other thermodynamic parameters in the basic thermodynamic Equation (9):

$$\Delta G_A = \Delta H_A - T\Delta S_A \quad (5)$$

where ΔH_A and ΔS_A are, respectively, the enthalpy and entropy of adsorption of the probe on the sample and T is the absolute temperature of columns. ΔH_A and ΔS_A can be obtained from the slope and intercept of the linear plot of $\Delta G_A/T$ against 1/T, assuming that both ΔH_A and ΔS_A remain invariant over the temperature range of interest.

The surface free energies of adsorption ($-\Delta G_A$) of MSX, SX-I, and SX-II for both the NPs and PPs were calculated from Eq. 2 and are tabulated in Table I. The corresponding enthalpy and entropy of adsorption calculated using Eq. (5) are shown in Table II.

Dispersive Component of Surface Free Energy and Related Thermodynamic Parameters

For the adsorption of NPs (alkane) involving purely dispersive forces, the work of adhesion is given by:

$$W_A = 2 (\gamma_S^D)^{1/2} (\gamma_L^D)^{1/2} \quad (6)$$

where γ_S^D is the dispersive component of surface free energy of the sample and γ_L^D is the dispersive component of surface free energy of the liquid probes.

Combining Eqs. (3), (4), and (6) affords the following :

$$RT \ln V_N = 2 a N (\gamma_S^D)^{1/2} (\gamma_L^D)^{1/2} + K_c \quad (7)$$

where the constant K_c takes into account the choice of the standard state of ΔG_A and the surface area of the sample (cf. Eq. 2).

Plot of RT ln V_N against a $(\gamma_L^D)^{1/2}$ according to Eq. 7 yields a linear slope of 2 N $(\gamma_S^D)^{1/2}$, from which the dispersive component of surface free energy of adsorption, γ_S^D, can be determined (7).

As with Eq. 5, the surface free energy G_S of the sample is related to its surface enthalpy H_S and surface entropy S_S as follows (10):

$$G_S = H_S - T S_S \quad (8)$$

Since the sample remains physically unchanged during the experiment, G_S may be equated to γ_S, and Eq. 8 can be expressed as:

$$\gamma_S = H_S - T S_S \quad (9)$$

If only dispersive forces are involved, Eq. 9 may be rewritten as follows:

$$\gamma_S^D = H_S^D - T S_S^D \quad (10)$$

where H_S^D and S_S^D are the dispersive components of surface enthalpy and surface entropy, respectively.

The surface free energies for the dispersive component, γ_S^D, of the MSX, SX-I, and SX-II samples at various temperatures are presented in Table III. The dispersive components of surface enthalpy (H_S^D) and surface entropy (S_S^D) of the samples also are tabulated in Table III.

Table I. Surface Free Energies of Adsorption ($-\Delta G_A$) of MSX, SX-I, and SX-II[a]

Probes	Samples	$-\Delta G_A$ (kJ/mol) 30°C	40°C	50°C	60°C
NPs					
Pentane	MSX	11.11 (0.24)	10.39 (0.17)	9.67 (0.19)	9.13 (0.23)
	SX-I	11.14 (0.73)	10.38 (0.72)	9.67 (0.69)	9.19 (0.71)
	SX-II	16.60 (0.24)	16.15 (0.27)	16.69 (0.18)	16.41 (0.24)
Hexane	MSX	13.81 (0.15)	13.03 (0.12)	12.25 (0.12)	11.57 (0.17)
	SX-I	13.68 (0.72)	12.86 (0.72)	12.08 (0.71)	11.49 (0.68)
	SX-II	18.98 (0.23)	18.46 (0.22)	18.84 (0.18)	18.43 (0.23)
Heptane	MSX	16.52 (0.10)	15.66 (0.11)	14.79 (0.10)	14.02 (0.11)
	SX-I	16.16 (0.70)	15.27 (0.70)	14.41 (0.68)	13.68 (0.69)
	SX-II	21.39 (0.24)	20.77 (0.21)	20.98 (0.17)	20.48 (0.22)
Octane	MSX	19.26 (0.05)	18.33 (0.10)	17.36 (0.06)	16.49 (0.08)
	SX-I	18.69 (0.71)	17.71 (0.70)	16.76 (0.67)	15.93 (0.67)
	SX-II	23.77 (0.22)	23.08 (0.22)	23.12 (0.18)	22.53 (0.22)
Nonane	MSX	–	–	–	–
	SX-I	20.93 (0.47)	20.22 (0.69)	19.17 (0.67)	18.24 (0.68)
	SX-II	25.86 (0.22)	25.35 (0.20)	25.22 (0.20)	24.56 (0.21)
PPs					
Dichloro-	MSX	–	–	–	–
methane	SX-I	12.41 (0.83)	11.94 (0.86)	11.70 (0.95)	11.70 (1.03)
	SX-II	21.51 (0.19)	21.10 (0.22)	21.71 (0.20)	21.38 (0.21)
Chloroform	MSX	14.78 (0.24)	14.06 (0.17)	13.32 (0.18)	12.61 (0.19)
	SX-I	14.03 (0.75)	13.19 (0.78)	12.45 (0.74)	11.87 (0.72)
	SX-II	23.65 (0.21)	23.16 (0.21)	23.67 (0.18)	23.26 (0.22)
Acetone	MSX	15.24 (0.08)	14.14 (0.13)	13.14 (0.16)	12.46 (0.26)
	SX-I	14.40 (0.33)	13.46 (0.49)	12.30 (0.13)	11.81 (0.43)
	SX-II	20.67 (0.20)	19.95 (0.13)	20.49 (0.09)	20.10 (0.17)
Ethyl	MSX	17.46 (0.06)	16.40 (0.13)	15.27 (0.14)	14.24 (0.12)
acetate	SX-I	15.87 (0.42)	14.96 (0.24)	13.77 (0.47)	13.02 (0.41)
	SX-II	22.53 (0.16)	21.94 (0.21)	22.28 (0.17)	21.79 (0.20)
Diethy ether	MSX	14.20 (0.11)	12.91 (0.13)	11.73 (0.13)	10.67 (0.16)
	SX-I	12.65 (0.44)	11.65 (0.36)	10.79 (0.41)	10.10 (0.41)
	SX-II	18.33 (0.17)	17.82 (0.21)	18.25 (0.16)	17.88 (0.18)
Tetrahydro-	MSX	17.02 (0.15)	16.08 (0.16)	15.12 (0.15)	14.18 (0.16)
furan	SX-I	15.83 (0.43)	14.77 (0.45)	13.82 (0.37)	13.13 (0.33)
	SX-II	22.87 (0.18)	22.40 (0.20)	22.90 (0.17)	22.54 (0.21)

[a] SDs are shown in parentheses.

Specific Interactions and Associated Acid-Base Properties

PPs have both dispersive and specific components of surface free energy of adsorption. The specific component of surface free energy of adsorption (ΔG_A^{SP}) is determined by subtracting the dispersive contribution from the total free energy of adsorption, and can be obtained from the vertical distance between the alkane reference line (Equation 7) and the PP of interest according to the following Eq. (7):

$$-\Delta G_A^{SP} = RT \ln (V_N/V_N^{ref}) \quad (11)$$

As before, ΔG_A^{SP} is related to the enthalpy (ΔH_A^{SP}) and entropy (ΔS_A^{SP}) of specific interactions in adsorption by:

$$\Delta G_A^{SP} = \Delta H_A^{SP} - T\,\Delta S_A^{SP} \quad (12)$$

The determined $-\Delta G_A^{SP}$ values together with the ΔH_A^{SP} and ΔS_A^{SP} obtained by linear regression of $\Delta G_A^{SP}/T$ against 1/T for MSX, SX-I, and SX-II are summarized in Table IV.

The PPs can be described in terms of the Gutmann electron donor (DN) and electron acceptor numbers (AN). DN defines the basicity or electron donor ability of a probe, while AN defines the acidity or electron acceptor ability. AN*, introduced by Fowkes (11), is a more appropriate quantity to use than AN since it is corrected for the contribution from the dispersive forces. DN and AN* can be related to the enthalpy of adsorption for specific interactions as follows (7):

$$-\Delta H_A^{SP} = K_A\,DN + K_D\,AN^* \quad (13a)$$

Or

$$-\Delta H_A^{SP}/AN^* = K_A\,(DN/AN^*) + K_D \quad (13b)$$

where K_A and K_D are numbers describing the acid and base characteristics of the solid (SX).

The values of DN and AN* of the liquid probes used can be obtained from the literature (12,13). Plotting $-\Delta H_A^{SP}/AN^*$ against DN/AN* yields a straight line where K_A and K_D correspond to slope and intercept, respectively.

Since the IGC free-energy terms can be determined more quickly and precisely than the enthalpic terms, it has become a common practice to employ ΔG_A^{SP} instead of ΔH_A^{SP} to estimate the acid-base properties of the crystal surface by assuming that the entropic contribution is negligible, and Eq. 13b is rewritten as (14,15):

Table II. Enthalpy and Entropy of Adsorption of MSX, SX-I, and SX-II[a]

Adsorption	MSX	SX-I	SX-II
NPs			
Pentane			
ΔH_A (kJ/mol)	−31.33	−30.99	−16.68
	(0.59)	(2.42)	(0.54)
ΔS_A (JK/mol)	−67 (2)	−66 (7)	−1 (1)
Hexane			
ΔH_A (kJ/mol)	−36.58	−35.96	−22.75
	(0.49)	(2.05)	(0.36)
ΔS_A (JK/mol)	−75 (2)	−74 (6)	−13 (1)
Heptane			
ΔH_A (kJ/mol)	−41.91	−41.31	−29.02
	(0.04)	(1.35)	(0.67)
ΔS_A (JK/mol)	−84 (0)	−83 (3)	−26 (2)
Octane			
ΔH_A (kJ/mol)	−47.45	−46.71	−34.86
	(0.36)	(1.43)	(0.41)
ΔS_A (JK/mol)	−93 (1)	−93 (3)	−37 (1)
Nonane			
ΔH_A (kJ/mol)	–	−51.66	−38.57
		(0.24)	(1.45)
ΔS_A (JK/mol)	–	−100 (2)	−42 (5)
PPs			
Dichloromethane			
ΔH_A (kJ/mol)	–	−19.71	−20.76
		(1.79)	(0.43)
ΔS_A (JK/mol)	–	−24 (8)	2 (1)
Chloroform			
ΔH_A (kJ/mol)	−36.72	−35.96	−25.56
	(0.93)	(1.74)	(1.00)
ΔS_A (JK/mol)	−72 (3)	−73 (4)	−7 (3)
Acetone			
ΔH_A (kJ/mol)	−43.59	−41.55	−24.14
	(1.93)	(5.84)	(1.98)
ΔS_A (JK/mol)	−94 (7)	−90 (18)	−12 (6)
Ethyl acetate			
ΔH_A (kJ/mol)	−50.17	−45.48	−28.14
	(0.58)	(1.93)	(0.44)
ΔS_A (JK/mol)	−108 (2)	−98 (6)	−19 (2)
Diethyl ether			
ΔH_A (kJ/mol)	−49.95	−38.57	−21.15
	(0.36)	(2.13)	(0.66)
ΔS_A (JK/mol)	−118 (2)	−86 (7)	−10 (2)
Tetrahydrofuran			
ΔH_A (kJ/mol)	−45.80	−43.37	−24.28
	(0.51)	(1.60)	(0.15)
ΔS_A (JK/mol)	−95 (2)	−91 (4)	−5 (1)

[a] SDs are shown in parentheses.

$$-\Delta G_A{}^{SP}/AN^* = K_A\,(DN/AN^*) + K_D \qquad (14)$$

The K_A and K_D values calculated from Eqs. 13 and 14 for MSX, SX-I, and SX-II are tabulated in Table V.

Hansen Solubility Parameters

The (Hildebrand) solubility parameter, δ, of a liquid is defined as the square root of the cohesive energy density by (16,17):

$$\delta = (E/V)^{1/2} \qquad (15)$$

Table III. Dispersive Components of Surface Free Energy of Adsorption and Related Thermodynamic Properties of MSX, SX-I and SX-II[a]

Components	MSX	SX-I	SX-II
γ_S^D at 30°C	40.49	34.55	31.10
(mJ/m^2)	(1.96)	(0.16)	(1.05)
γ_S^D at 40°C	38.29	32.48	28.56
(mJ/m^2)	(0.91)	(0.25)	(1.11)
γ_S^D at 50°C	35.77	30.22	24.57
(mJ/m^2)	(1.00)	(0.24)	(0.88)
γ_S^D at 60°C	32.90	27.39	22.43
(mJ/m^2)	(1.29)	(0.90)	(0.66)
S_S^D	0.253	0.237	0.300
(mJ/m^2/K)	(0.037)	(0.033)	(0.016)
H_S^D	117.33	106.67	122.05
(mJ/m^2)	(12.65)	(10.20)	(5.97)

[a] SDs are shown in parentheses.

where V is the molar volume of the liquid, and E is its (measurable) energy of vaporization.

The premise of the Hansen solubility parameters is that the total energy of the vaporization of the liquid consists of individual parts arising from (atomic) dispersion force, (molecular) permanent dipole-permanent dipole forces, and (molecular) hydrogen bonding (electron-exchange) (16,17). Thus,

$$E = E_D + E_P + E_V \qquad (16)$$

Dividing Eq. 16 by the molar volume, V, affords the square of the total (Hildebrand) solubility parameter ($\delta_T{}^2$) as the sum of the squares of Hansen component parameters for dispersive forces ($\delta_D{}^2$), polar interactions ($\delta_P{}^2$), and hydrogen bonding ($\delta_H{}^2$), that is,

$$E/V = E_D/V + E_P/V + E_V/V \qquad (17a)$$

$$\delta_T{}^2 = \delta_D{}^2 + \delta_P{}^2 + \delta_H{}^2 \qquad (17b)$$

It must be noted that Eqs. 15–17, being based on liquids, are not applicable to solids, which tend to decompose before vaporization. However, using the model developed by Karger *et al.* (18), the Hansen solubility parameters of solids can be calculated from IGC data.

In IGC, the experimental parameter, V_N, can be linked to the Hansen solubility parameters through Eqs. 18 and 19 given below. Dividing V_N by the mass of the sample affords the specific retention volume, V_G, which can be related to the transfer energy of adsorption, ΔE^A, for polar systems as follows:

$$\ln V_G = -(\Delta E^A/RT) + K_G \qquad (18)$$

where R is the gas constant, T is the absolute temperature, and K_G is a constant. In this case, ΔE^A, calculated from a plot of ln V_G vs. 1/T, is equivalent to the enthalpy of adsorption, ΔH_A.

ΔE^A is related to the Hansen solubility parameters by the following Eq. (19):

$$-\Delta E^A = V_P\,(\delta_D{}^P\,\delta_D{}^S + \delta_P{}^P\,\delta_P{}^S + \delta_H{}^P\,\delta_H{}^S) \qquad (19)$$

where V_P is the molar volume of the probe; $\delta_D{}^P$, $\delta_P{}^P$, and $\delta_H{}^P$ are the Hansen partial solubility parameters of the probes for the dispersion component, polar forces, and hydrogen-

Table IV. Specific Components of Surface Free Energy of Adsorption of MSX, SX-I, and SX-II[a]

Components	Dichloromethane	Chloroform	Acetone	Ethyl acetate	Diethyl ether	Tetrahydrofuran
$-\Delta G_A^{SP}$ at 30°C (kJ/mol)						
MSX	–	0.73 (0.10)	4.97 (0.18)	4.29 (0.12)	3.37 (0.12)	3.78 (0.03)
SX-I	2.57 (0.11)	0.16 (0.05)	4.02 (0.98)	2.81 (0.36)	1.75 (0.39)	2.71 (0.34)
SX-II	6.14 (0.13)	4.46 (0.03)	4.78 (0.10)	4.11 (0.10)	1.96 (0.06)	4.38 (0.11)
$-\Delta G_A^{SP}$ at 40°C (kJ/mol)						
MSX	–	0.81 (0.05)	4.56 (0.10)	4.00 (0.01)	2.77 (0.04)	3.61 (0.03)
SX-I	2.81 (0.15)	0.15 (0.08)	3.80 (1.17)	2.71 (0.61)	1.49 (0.39)	2.45 (0.28)
SX-II	6.11 (0.17)	4.50 (0.13)	4.47 (0.15)	4.02 (0.11)	1.86 (0.06)	4.42 (0.14)
$-\Delta G_A^{SP}$ at 50°C (kJ/mol)						
MSX	–	0.87 (0.04)	4.24 (0.02)	3.63 (0.03)	2.29 (0.05)	3.42 (0.01)
SX-I	3.22 (0.25)	0.20 (0.06)	3.31 (0.84)	2.27 (0.23)	1.32 (0.33)	2.26 (0.35)
SX-II	6.10 (0.17)	4.65 (0.12)	4.41 (0.13)	3.95 (0.12)	1.74 (0.07)	4.51 (0.11)
$-\Delta G_A^{SP}$ at 60°C (kJ/mol)						
MSX	–	0.83 (0.05)	4.08 (0.20)	3.25 (0.10)	1.78 (0.11)	3.12 (0.08)
SX-I	3.65 (0.37)	0.23 (0.08)	3.28 (1.11)	2.10 (0.35)	1.09 (0.33)	2.15 (0.46)
SX-II	6.01 (0.15)	4.65 (0.11)	4.30 (0.12)	3.83 (0.10)	1.66 (0.08)	4.52 (0.11)
ΔH_A^{SP} (kJ/mol)						
MSX	–	0.37 (1.13)	–14.02 (2.75)	–14.81 (0.99)	–19.25 (1.11)	–10.31 (0.88)
SX-I	8.38 (2.54)	0.61 (0.41)	–12.30 (8.10)	–10.61 (1.95)	–8.24 (1.17)	–8.36 (1.24)
SX-II	–7.33 (0.04)	–2.25 (0.77)	–9.38 (1.64)	–6.81 (0.53)	–5.11 (0.37)	–2.79 (0.36)
ΔS^{SP} (JK/mol)						
MSX	–	4 (4)	–30 (9)	–35 (3)	–52 (3)	–21 (3)
SX-I	36 (9)	2 (1)	–27 (25)	–26 (5)	–21 (3)	–19 (5)
SX-II	330 (578)	317 (536)	311 (562)	325 (577)	319 (569)	332 (565)

[a] SDs are shown in parentheses.

bonding, respectively; and δ_D^S, δ_P^S, and δ_H^S are the corresponding Hansen solubility parameters for the solid samples, which can be obtained by multiple linear regression through origin using known δ_D^P, δ_P^P, and δ_H^P values of the probes from the literature.

The Hansen solubility parameters of the SX samples determined by IGC are shown in Fig. 1.

RESULTS AND DISCUSSION

Standard Free Energy of Adsorption and Related Thermodynamic Parameters

As shown in Table I, the free energies of adsorption ($-\Delta G_A$) of all NPs in the alkane series obtained at various temperatures for the three SX samples followed this order: SX-II > MSX ≈ SX-I, suggesting that the adsorption of the alkane probes is energetically similar toward MSX and SX-I, but thermodynamically more favorable on SX-II. Analysis of the temperature dependence of ΔG_A for the SX samples revealed that the MSX and SX-I had statistically equivalent ΔH_A and ΔS_A and hence comparable $-\Delta G_A$, whereas SX-II had a less negative ΔH_A and a much less negative ΔS_A than MSX and SX-I, the net result being a higher $-\Delta G_A$ for SX-II (Table II). In other words, the more favorable adsorption of the NP on SX-II is driven by a considerably reduced loss in surface entropy (disorder or molecular mobility). The measured ΔS_A values of MSX, SX-I, and SX-I are of the same order of magnitude as the predicted entropy changes (based on ideal gas behavior) for adsorption of heptane, octane, and nonane (–52.4, –53.0, and –53.5 JK/mol, respectively, at 20°C), as reported in the literature (20). The higher than predicted entropy loss of the alkanes upon adsorption on MSX and

Table V. K_A and K_D Values of MSX, SX-I, and SX-II[a]

Values	MSX	SX-I	SX-II
From $-\Delta H_A^{SP}$ K_A	0.399	0.432	0.102
	(0.039)	(0.050)	(0.019)
K_D	5.295	0.213	2.077
	(0.786)	(0.891)	(0.267)
K_D/K_A	13.271	0.493	20.363
From $-\Delta G_A^{SP}$ at 30°C			
K_A	0.179	0.123	0.188
	(0.001)	(0.016)	(0.005)
K_D	0.413	0.326	0.612
	(0.044)	(0.064)	(0.014)
K_D/K_A	2.307	2.650	3.255
From $-\Delta G_A^{SP}$ at 40°C			
K_A	0.172	0.110	0.191
	(0.001)	(0.013)	(0.006)
K_D	0.298	0.356	0.554
	(0.021)	(0.120)	(0.013)
K_D/K_A	1.733	3.236	2.901
From $-\Delta G_A^{SP}$ at 50°C			
K_A	0.163	0.100	0.195
	(0.001)	(0.017)	(0.005)
K_D	0.204	0.329	0.508
	(0.013)	(0.020)	(0.019)
K_D/K_A	1.252	3.290	2.605
From $-\Delta G_A^{SP}$ at 60°C			
K_A	0.148	0.093	0.196
	(0.003)	(0.022)	(0.005)
K_D	0.158	0.347	0.467
	(0.026)	(0.035)	(0.020)
K_D/K_A	1.068	3.731	2.383

[a] SDs are shown in parentheses.

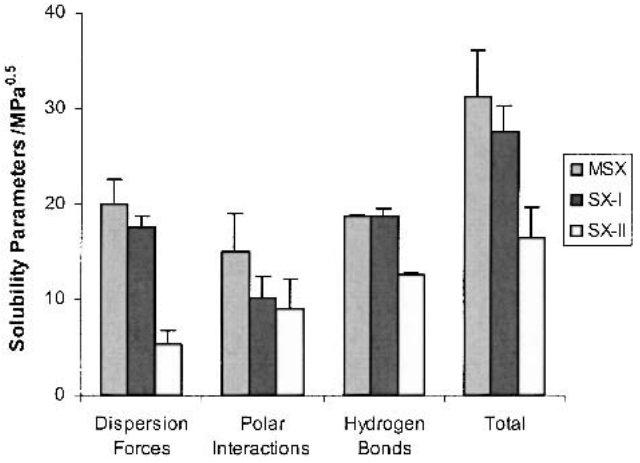

Fig. 1. Hansen solubility parameters determined by IGC for MSX, SX-I, and SX-II.

SX-I may be explained by the loss of one degree of translational freedom and by a restriction of rotational and vibrational freedom on the surface. In contrast, the entropy loss associated with the adsorption of alkane probes on SX-II was much lower than predicted, suggesting that the adsorbed probe molecules still retain much of their mobility on the surface of SX-II. The less negative ΔH_A obtained with SX-II, which indicated less heat being evolved through bond formation during the adsorption, may be explained by weaker interactions resulting from a reduced number of nonpolar binding sites and the increased mobility of the probe molecules.

For the PPs, the $-\Delta G_A$ values of the three SX samples decreased in the order SX-II > MSX > SX-I, although MSX showed only a marginally higher $-\Delta G_A$ than SX-I (Table I). Analysis of the surface free energy of the samples in terms of enthalpic and entropic contributions also revealed that SX-II afforded a less negative ΔH_A and a substantially less negative ΔS_A than MSX or SX-I, which is similar to the case with the NPs (Table II). This again suggests that a much reduced loss in entropy (or increased molecular mobility) rather than a major loss in enthalpy is the driving force for the more favorable adsorption of the PPs on SX-II, which is apparently linked to the less stable and more disordered form II structure. However, unlike the case with the NPs, the ΔH_A and ΔS_A values of MSX for the PPs displayed some differences from those of SX-I, although only the data obtained for ethyl acetate and diethyl ether were statistically significantly different. For these probes, MSX had a more negative ΔH_A and a somewhat more negative ΔS_A than SX-I. Thus, it would appear that the slightly higher $-\Delta G_A$ of MSX relative to SX-I is contributed mainly by a more negative ΔH_A, possibly resulting from an increased number and strength of high-energy binding sites. As discussed previously, micronization can increase the surface free energy of SX by introducing structural defects or by exposing more polar groups (i.e., binding sites) at the particle surface (5).

Dispersive Component of Surface Free Energy and Related Thermodynamic Parameters

The dispersive component of surface free energy, γ_S^D, determined from the whole nonpolar alkane series for each sample at various temperatures decreased in the following order for the three SX samples: MSX > SX-I > SX-II (which was the reverse sequence of that expressed by the $-\Delta G_A$ values; Table III). According to Eqs. 4, 6, and 7, the trend of $-\Delta G_A$ should closely parallel that of γ_S^D provided that the constant term K in Eq. 4 (the magnitude of which depends on the reference standard state used for ΔG_A) is zero or equivalent for all the SX samples. However, while the plot of $-\Delta G_A$ vs. $a(\gamma_L^D)^{1/2}$ afforded excellent linearity ($r \approx 0.99$) for all the SX samples, the intercept value was statistically indistinguishable for MSX and SX-I, but considerably higher for SX-II than for MSX and SX-I (by about –7.1 and –6.1 kJ/mol, respectively, at 30°C). This substantial additional $-\Delta G_A$ change for SX-II, which is not explicable by purely dispersive interactions, is likely a result of the increased mobility of the probe molecules on the less stable and more disordered SX-II surface, as discussed earlier. Thus, although the SX-II showed the largest $-\Delta G_A$, its γ_S^D was the smallest, reflecting a relatively low contribution of the dispersive (nonpolar) forces on a predominantly polar and relatively disordered surface. That MSX has a higher γ_S^D than the SEDS-processed SX-I may be explained by the less crystalline or more defective surface of the MSX sample, as alluded to earlier.

Examination of γ_S^D in terms of the enthalpic and entropic contributions revealed that the H_S^D and S_S^D were the highest for SX-II, followed by MSX and then by SX-I (Table III). This is consistent with the fact that the SX-II is the metastable polymorph at ambient temperature and has a higher surface enthalpy and entropy than SX-I, while the SEDS-processed SX-I is more crystalline than MSX and is characterized by a lower surface enthalpy and entropy. The relatively low γ_S^D observed for SX-II is mainly related to its higher surface entropy.

Specific Interactions and Associated Acid-Base Properties

The $-\Delta G_A^{SP}$ values of SX-II determined at various temperatures for all the PPs were considerably higher than those of SX-I, particularly for the acidic probes (dichloromethane and chloroform), reflecting more thermodynamically favorable adsorption of these PPs on SX-II (Table IV). The higher $-\Delta G_A^{SP}$ observed with the adsorption of polar acidic probes on SX-II also suggests that the surface of SX-II exhibits predominantly specific basic interactions. As before, the free energy change was further analyzed in terms of enthalpy and entropy. The ΔS_A^{SP} values determined from ΔG_A^{SP} at various temperatures were highly variable, particularly for the SX-II sample, while the calculated ΔH_A^{SP} generally showed acceptable consistency (i.e., reasonably low standard deviations) for statistical comparison. The observed data variability with ΔS_A^{SP} and, to a slight degree, ΔH_A^{SP} is mainly due to the involvement of multiple calculation steps in arriving at these data. These steps include: (1) construction of the alkane reference line based on retention volume data ($\ln V_N$) of the NPs; (2) subtraction of the $\ln V_N$ data of the PPs from the corresponding $\ln V_N$ values for the NPs on the reference line to afford ΔG_A^{SP}; and (3) linear regression of $\Delta G_A^{SP}/T$ against 1/T to obtain ΔH_A^{SP} and ΔS_A^{SP} (see Eq. 12). Each step can introduce significant errors, particularly in the second step where the difference of $\ln V_N$ measured constitutes a relatively small percentage of the respective $\ln V_N$ data. All of these errors would be cumulatively reflected in the final re-

sults. Thus, while the high $-\Delta G_A^{SP}$ of SX-II appeared to be contributed mainly by its high ΔS_A^{SP}, the dominance of the entropy factor in the adsorption process could not be statistically verified due to the considerable variability of the ΔS_A^{SP} data. Despite the difficulty in obtaining consistent ΔS_A^{SP} data for SX-II, the estimation of ΔH_A^{SP} was sufficiently robust to enable reliable comparison of the samples in terms of the nature of the specific interaction (i.e., dominant repulsive or attractive forces for the specific polar groups) involved in the adsorption. As already established, the total enthalpy of adsorption of the PP (ΔH_A) on the samples is negative (Table II). This follows from the fact that the total ΔG_A (Table I) for any spontaneous adsorption process is negative and that the ΔS_A is necessarily negative according to Eq. 5 (Table II) because the probe molecules in the vapor phase should have a larger entropy than those adsorbed on the crystal surfaces. However, the specific (polar) part of the enthalpy calculated using Eq. 12 can be either negative or positive. As presented in Table IV, both SX-I and SX-II exhibited negative ΔH_A^{SP} for the polar amphoteric (acetone and ethyl acetate) and basic (diethyl ether and tetrahydrofuran) probes, suggesting attractive specific interactions. In addition, the ΔH_A^{SP} of SX-I was more negative than that of SX-II, indicating stronger attractive forces of adsorption for these probes on SX-I. However, for the polar acidic probes, the ΔH_A^{SP} values determined for MSX (with chloroform) and SX-I (with chloroform and dichloromethane) were positive, although the overall free energy change observed at various temperatures was still negative, implying that the adsorption involves repulsive forces, possibly between similar chemical groups carrying like charges (i.e., between acidic groups in this case). The above observations suggest that the surface of SX-I involves predominantly acidic forces (from acidic groups), whereas the SX-II surface is characterized mainly by basic forces (from basic groups). Compared with the SEDS-processed SX-I, MSX exhibited a higher $-\Delta G_A^{SP}$ for all the PPs, which was attributable to its more negative ΔH_A^{SP} since the ΔS_A^{SP} values were statistically indistinguishable for all the PPs (except for the basic diethyl ether probe). The more negative ΔH_A^{SP} values with MSX relative to the SEDS SX-I for the various PPs are indicative of stronger specific acidic and basic forces of interaction (21), possibly resulting from structural defects that expose more acidic and basic functional groups at the surface.

The strength and relative contribution of the acidic and basic forces were further analyzed by determining the acid and base numbers, K_A and K_D, of the samples. These numbers describe the acid and base properties of the materials and can be calculated from either ΔG_A^{SP} or ΔH_A^{SP} (Eqs. 13 and 14). Fundamentally, it is more appropriate to calculate K_A and K_D from ΔH_A^{SP} since the latter quantity directly reflects intermolecular interactions and the assumption of negligible ΔS_A^{SP} need not be considered. However, as explained earlier, the determination of ΔH_A^{SP} requires IGC measurements at multiple temperatures and may be subject to considerable experimental and computational errors, while the estimation of ΔG_A^{SP} involves measurement at only one defined temperature and can be accomplished more readily and precisely. For this reason, ΔG_A^{SP} is commonly employed for estimating K_A and K_D. As shown in Table V, the K_A and K_D based on ΔG_A^{SP} at various temperatures were higher for SX-II than for SX-I, whereas the K_A was higher for MSX than for SX-I, but the K_D was lower for MSX than for SX-I. This suggests that SX-II is more surface energetic than SX-I with respect to both basic and acidic forces, while the acidic forces account mostly for the higher surface energy of MSX relative to SX-I. The ratio of K_D to K_A (which determines the relative contribution of the basic and acidic properties in each sample) for the various SX samples generally followed the order SX-I > SX-II > MSX, suggesting that the basic forces are more dominant by proportion on the surface of SX-I than on the surfaces of SX-II and MSX. In contrast, the K_A and K_D values obtained from ΔH_A^{SP} showed considerable differences in magnitude and trend from those based on ΔG_A^{SP} among the three samples. The enthalpy-based K_A value was comparable for MSX and the SEDS SX-I but was much higher for SX-I than for SX-II, indicating relatively weak acidic forces of interactions on the surface of SX-II. On the other hand, the enthalpy-based K_D value was the highest for MSX, followed sequentially by SX-II and SX-I, suggesting that the surfaces of MSX and SX-II are predominated by relatively strong basic forces compared with SX-I. In addition, the calculated K_D/K_A ratios of MSX and SX-II were 13.2 and 20.3, respectively, reflecting an overwhelmingly large contribution of basic forces on the surfaces of these samples. However, the K_D/K_A ratio of SX-I was less than unity, implying a relative preponderance of the acidic forces on its surface. These latter findings accord with those deduced directly from the ΔH_A^{SP} data but contrast sharply with those inferred from the free-energy-based K_A and K_D, and they highlight the importance of accounting for the contribution of ΔS_A^{SP} in the calculation of the acid and base numbers.

Hansen Solubility Parameters

The concept of solubility parameters (or cohesive energy densities) and their applications to solubility prediction and surface characterization have been discussed elsewhere and will not be elaborated here (see Ref. 6 for review). Solubility parameters are derived from the cohesive energy of a material, which is the energy required to bind its constituent atoms or molecules together, and is dependent on the types of interatomic or intermolecular interactions involved. Though strictly a bulk thermodynamic property, solubility parameters have found wide application in material surface characterization, and specifically, in the quantitation of the relative contribution and strength of the dispersive and specific surface interactions for polar materials. Such applications are conditional on an established relationship between solubility parameter (or cohesive energy) and surface energy. However, as has been widely recognized, the surface of a material (particularly a highly crystalline solid) is not necessarily predictable from its bulk energetics, and *vice versa*, since the former is relatively prone to variation, depending on the way by which the material is prepared or processed, and the external environment with which it comes into contact. Thus, solubility parameters derived from surface energy measurements, although useful for surface characterization purposes, may carry very little predictive information on the bulk energetic state of a material.

In the present study, the total (Hildebrand) and the individual Hansen solubility parameters for various nonpolar and polar surface component forces of the SX samples were determined by IGC at infinite dilution. Presented in Fig. 1 are

the Hansen solubility parameters determined by IGC for the various SX samples. For each sample, the total solubility parameter (δ_T) calculated from IGC data was resolved into three separate component parameters for the dispersive forces (δ_D), polar forces (δ_P), and hydrogen bonding (δ_H) by multiple linear regression (through origin) analysis (r = 0.94–0.99; n = 11).

Comparison of the various measured solubility parameters between MSX and SX-I revealed statistically comparable values of δ_D, δ_P, δ_H, and δ_T for the two samples, although the solubility parameters on the dispersive and polar forces (i.e., δ_D and δ_P) tended to be higher for MSX. This observation is in close agreement with the more negative ΔH_A, higher γ_S^D, and more negative ΔH_A^{SP} displayed by the MSX sample. The percentage contributions of the dispersive, polar, and hydrogen-bonding forces to the overall surface energetics calculated from solubility parameters (by dividing the square of each component parameter by that of the total) were 41%, 23%, and 36%, respectively, for MSX and 40.4%, 13.3%, and 46.3% for SX-I, indicating roughly comparable contributions from nonpolar (41%) and specific (59%) interactions for both SX samples. On the other hand, SX-II exhibited lower solubility parameters for all the components (particularly for δ_D and δ_H) than did both MSX and SX-I, which is consistent with the less negative ΔH_A, the lower γ_S^D, and the less negative ΔH_A^{SP} values of SX-II. The substantial differences in solubility parameters between SX-II and SX-I or MSX are largely attributable to the differences in crystal structure between the two forms, which govern intermolecular bonding and hence the exposed functional groups at each crystal face. As discussed earlier, while the adsorption of NPs and PPs on SX-II is associated with a substantial free energy ($-\Delta G_A$) change, the major contribution actually derives from a much-reduced loss in entropy with the result that the heat release through bond formation is considerably decreased. Employing the same computational approach for SX-I and MSX as before, the percentage contributions of the dispersive, polar, and hydrogen-bonding forces to the total surface energetics were determined to be 10.6%, 30.8%, and 58.6%, respectively. These figures showed that the polar forces and hydrogen bonding together accounted for nearly 90% of the total surface energetics, reflecting an overwhelmingly polar surface, whereas the dispersive (nonpolar) forces constituted only a very minor contribution (10%), which is consistent with the relatively low γ_S^D value of SX-II. The dominant contribution of hydrogen bonding in SX-II suggests that the functional groups capable of forming hydrogen bonds (i.e., OH, COOH, and NH) are much larger in number or considerably more exposed at the surface than the relatively nonpolar benzene and naphthalene groups. These hydrogen-bonding groups are mostly the basic ones, that is, NH and CO, as implied by the high K_D value.

CONCLUSION

The present study clearly demonstrates that entropy plays an important role in the free energy change associated with surface intermolecular interactions for the two SEDS-processed SX polymorphs, particularly for the metastable form II (SX-II). For fundamental reasons and wherever feasible, comparison of the intermolecular forces involved in surface interactions should be based on enthalpy rather than free energy measurements since the former directly reflects intermolecular bonding.

Comparison of the surface interactions with the various NPs and PPs between SX-I and SX-II indicates that SX-II exhibits a higher $-\Delta G_A$ and $-\Delta G_A^{SP}$ (contributed by a much lower entropy loss during the adsorption), a smaller γ_S^D, a larger K_D (i.e., stronger basic forces), and a more prominent contribution of specific (polar) interactions. In contrast, MSX differs from SX-I mainly in having a larger $-\Delta G_A^{SP}$ (due to a greater heat loss during the adsorption), γ_S^D, and K_D. Thus, it can be concluded that the metastable SEDS SX-II polymorph possesses a higher surface free energy, a higher surface entropy, and a more polar surface than the stable SEDS SX-I polymorph, whereas the MSX displays a higher surface free energy and enthalpy than the SEDS SX-I material.

ACKNOWLEDGMENTS

Financial support was received from the Research Grant Council of Hong Kong (Earmarked Grant CUHK4244/98M).

REFERENCES

1. S. Palakodaty and P. York. Phase behavioral effects on particle formation processes using supercritical fluids. *Pharm. Res.* **16**: 976–985 (1999).
2. P. York. Strategies for particle design using supercritical fluid technologies. *Pharm. Sci. Technol. Today* **2**:430–440 (1999).
3. S. Beach, D. Latham, C. Sigdwick, M. Hanna, and P. York. Control of the physical form of salmeterol xinafoate. *Org. Process Res. Dev.* **3**:370–376 (1999).
4. A. D. Edwards, B. Yu. Shekunov, A. Kordikowski, R. T. Forbes and P. York. Crystallization of pure anhydrous polymorphs of carbamazepine by solution enhanced dispersion by supercritical fluids (SEDS) process. *J. Pharm. Sci.* **90**:1115–1124 (2001).
5. H. H. Y. Tong, B. Y. Shekunov, P. York, and A. H. L. Chow. Characterization of two polymorphs of salmeterol xinafoate crystallized from supercritical fluid. *Pharm. Res.* **18**:852–858 (2001).
6. B. C. Hancock, P. York, and R. C. Rowe. The use of solubility parameters in pharmaceutical dosage form design. *Int. J. Pharm.* **148**:1–21 (1997).
7. J. Schultz and L. Lavielle. Interfacial properties of carbon fiber-epoxy matrix composites. In D. R. Lloyd, T. C. Ward, H. P. Schreiber, and C. C. Pizana (eds.), *Inverse Gas Chromatography—Characterization of Polymers and Other Materials,* American Chemical Society, Washington, DC, 1989 pp. 185–202.
8. J. H. de Boer. *The Dynamic Character of Adsorption 2nd Ed,* Clarendon Press, Oxford, 1968.
9. S. J. Gregg. *The Surface Chemistry of Solids,* Whitefriars Press, London, 1965.
10. A. W. Adamson and A. P. Gast. *Physical Chemistry of Surfaces,* John Wiley & Sons, New York, 1997.
11. F. M. Fowkes. Quantitative characterisation of the acid-base properties of solvents, polymers, and inorganic surfaces. *J. Adhesion Sci. Technol.* **4**:669–691 (1990).
12. V. Gutmann. *The Donor-Acceptor Approach to Molecular Interactions*, Plenum Press, New York and London, 1978.
13. F. L. Riddle and F. M. Fowkes. Special shifts in acid-base chemistry: 1. Van der Waals contributions to acceptor numbers. *J. Am. Chem. Soc.* **112**:3260–3264 (1990).
14. J. C. Feeley, P. York, B. S. Sumby, and H. Dicks. Determination of surface properties and flow characteristics of salbutamol sulphate, before and after micronisation. *Int. J. Pharm.* **172**:89–96 (1998).
15. M. D. Ticehurst, R. C. Rowe, and P. York. Determination of the surface properties of two batches of salbutamol sulphate by inverse gas chromatography. *Int. J. Pharm.* **111**:241–249 (1994).
16. C. M. Hansen. *Hansen Solubility Parameters – A User's Handbook,* CRC Press, Boca Raton, Florida, 2000.

17. A. F. M. Barton. *Handbook of Solubility Parameters and Other Cohesion Parameters,* CRC Press, Boca Raton, Florida, 1991.
18. B. L. Karger and L. R. Snyder, and C. Eon. Expanded solubility parameter treatment for classification and use of chromatographic solvents and adsorbents. *Anal. Chem.* **50**:2126–2136 (1978).
19. N. Huu-Phouc, R. P. T. Luu, A. Munafo, P. Ruelle, H. Nam-Tran, M. Buchmann, and U. W. Kesselring. Determination of partial solubility parameters of lactose by gas-solid chromatography. *J. Pharm. Sci.* **75**:68–72 (1986).
20. S. Katz and D. G. Gray. The adsorption of hydrocarbons of cellophane: I. Zero surface coverage. *J. Colloid Interface Sci.* **82**: 318–325 (1980).
21. E. Papirer, E. Brendle, H. Balard, and C. Vergelati. Inverse gas chromatography investigation of the surface properties of cellulose. *J. Adhesion Sci. Technol.* **14**:321–337 (2000).